

1  
2  
3  
4  
5  
6  
7  
8  
9  
10  
11  
12  
13  
14  
15  
16  
17  
18  
19  
20  
21  
22  
23  
24

**Hydraulic and transport parameter assessment using column infiltration experiments**

A. Younes<sup>1,2,3</sup>, T.A. Mara<sup>4</sup>, M. Fahs<sup>1</sup>, O. Grunberger<sup>2</sup>, Ph. Ackerer<sup>\*,1</sup>

<sup>1</sup> LHyGES, Université de Strasbourg/ENGEEES, CNRS, 1 rue Blessig, 67084 Strasbourg, France.

<sup>2</sup> IRD UMR LISAH, F-92761 Montpellier, France.

<sup>3</sup> LMHE, Ecole Nationale d'Ingénieurs de Tunis, Tunisie

<sup>4</sup> Université de La Réunion, PIMENT, 15 Avenue René Cassin, BP 7151, 97715 Moufia, La Réunion.

\* Contact person: Ph. Ackerer

E-mail: ackerer@unistra.fr

25 ***Abstract***

26 The quality of statistical calibration of hydraulic and transport soil properties is studied for  
27 infiltration experiments in which, over a given period, tracer-contaminated water is injected  
28 into an hypothetical column filled with a homogeneous soil. The saturated hydraulic  
29 conductivity, the saturated and residual water contents, the Mualem-van Genuchten shape  
30 parameters and the longitudinal dispersivity are estimated in a Bayesian framework using the  
31 Markov Chain Monte Carlo (MCMC) sampler. The impact of the kind of measurement sets  
32 (water content, pressure inside the column, cumulative outflow and outlet solute  
33 concentration) and that of the solute injection duration is investigated by analyzing the  
34 calibrated model parameters and their confidence intervals for different scenarios. The results  
35 show that the injection period has a significant effect on the quality of the estimation, in  
36 particular, on the posterior uncertainty range of the parameters. All hydraulic and transport  
37 parameters of the investigated soil can be well estimated from the experiment using only the  
38 outlet concentration and cumulative outflow, which are measured non-intrusively. An  
39 improvement of the identifiability of the hydraulic parameters is observed when the pressure  
40 data from measurements taken inside the column are also considered in the inversion.

41

42 **Keywords**

43 Infiltration experiment, Richards' equation, Statistical calibration, Markov Chain Monte  
44 Carlo, Uncertainty ranges.

45

## 46 **1. Introduction**

47 The soil parameters that influence water flow and contaminant transport in unsaturated zones  
48 are not generally known *a priori* and have to be estimated by fitting model responses to  
49 observed data. The unsaturated soil hydraulic parameters can be (more or less accurately)  
50 estimated from dynamic flow experiments (*e.g.*, Hopmans et al., 2002; Vrugt et al., 2003a;  
51 Durner and Iden, 2011; Younes et al., 2013). Several authors have investigated different types  
52 of transient experiments and boundary conditions suited for a reliable estimation of soil  
53 hydraulic properties (*e.g.* van Dam et al., 1994; Simunek and van Genuchten, 1997; Inoue et  
54 al, 1998; Durner et al, 1999). Soil hydraulic properties are often estimated using inversion of  
55 one-step (Kool et al., 1985; van Dam et al., 1992) or multistep (Eching et al., 1994; van Dam  
56 et al., 1994) outflow experiments or controlled infiltration experiments (Hudson et al., 1996).  
57 Kool et al. (1985) and Kool and Parker (1988) suggested that the transient experiments should  
58 cover a wide range in water contents to obtain a reliable estimation of the parameters. Van  
59 Dam et al. (1994) have shown that more reliable parameter estimates are obtained by  
60 increasing the pneumatic pressure in several steps instead of a single step. The multistep  
61 outflow experiments are the most popular laboratory methods (*e.g.*, Eching and Hopmans,  
62 1993; Eching et al., 1994; van Dam et al., 1994; Hopmans et al., 2002). However, their  
63 application is limited by expensive measurement equipment (Nasta et al., 2011).  
64 Infiltration experiments have been investigated by Mishra and Parker (1989) to study the  
65 reliability of hydraulic and transport estimated parameters for a soil column of 200 cm using  
66 measurements of water content, concentration and water pressure inside the column. They  
67 showed that the simultaneous estimation of hydraulic and transport properties yields to  
68 smaller estimation errors for model parameters than the sequential inversion of hydraulic  
69 properties from the water content and/or pressure head followed by the inversion of transport  
70 properties from concentration data (Mishra and Parker, 1989).

71 Inoue et al. (2000) performed infiltration experiments using a soil column of 30 cm. Pressure  
72 head and solute concentration were measured at different locations. A constant infiltration rate  
73 was applied to the soil surface and a balance was used to measure the cumulative outflow.  
74 They showed that both hydraulic and transport parameters can be assessed by the combination  
75 of flow and transport experiments.

76 Furthermore, infiltration experiments were often conducted in lysimeters for pesticide  
77 leaching studies. Indeed, lysimeter experiments are generally used to assess the leaching risks  
78 of pesticides using soil columns of around 1.2 m depth which is the standard scale for these  
79 types of experiments (Mertens et al, 2009; Kahl et al., 2015). Before performing the column  
80 leaching experiment, several infiltration-outflow experiments are often realized to estimate  
81 the soil hydraulic parameters (Kahl et al., 2015; Dusek et al, 2015).

82 The key objective of the present study is to evaluate the reliability of different experimental  
83 protocols for estimating hydraulic and transport parameters and their associated uncertainties  
84 for column experiments. We consider the flow and the transport of an inert solute injected  
85 into a hypothetical column filled with a homogeneous sandy clay loam soil. We assume that  
86 flow can be modelled by the Richards' equation (RE) and that the solute transport can be  
87 simulated by the classical advection-dispersion model. Furthermore, the Mualem and van  
88 Genuchten (MvG) models (Mualem 1976, van Genuchten 1980) are chosen to describe the  
89 retention curve and to relate the hydraulic conductivity of the unsaturated soil to the water  
90 content. The estimation of the flow and transport parameters through flow-transport model  
91 inversion is investigated for two injection periods of the solute and different data  
92 measurement scenarios.

93 Inverse modelling is often performed using local search algorithms such as the Levenberg-  
94 Marquardt algorithm (Marquardt, 1963). The later is computationally efficient to evaluate the  
95 optimal parameter set (Gallagher and Doherty, 2007). Besides, the degree of uncertainty in

96 the estimated parameters, expressed by their confidence intervals, is often calculated using a  
97 first-order approximation of the model near its minimum (Carrera and Neuman, 1986, Kool  
98 and parker, 1988). However, as stated by Vrugt and Bouten (2002), parameter  
99 interdependence and model nonlinearity occurring in hydrologic models may violate the use  
100 of this first approximation to obtain accurate confidence intervals of each parameter.  
101 Therefore, in this work, the estimation of hydraulic and transport parameters is performed in a  
102 Bayesian framework using the Markov Chain Monte Carlo (MCMC) sampler (Vrugt and  
103 Bouten, 2002; Vrugt et al., 2008). Unlike classical parameter optimization algorithms, the  
104 MCMC approach generates sets of parameter values randomly sampled from the posterior  
105 joint probability distributions, which are useful to assess the quality of the estimation. The  
106 MCMC samples can be used to summarize parameter uncertainties and to perform predictive  
107 uncertainty (Ades and Lu, 2003).

108 Hypothetical infiltration experiments are considered for a column of 120 cm depth, initially  
109 under hydrostatic conditions, free of solute and filled with a homogeneous sandy clay loam  
110 soil. Continuous flow and solute injection are performed during a time period  $T_{inj}$  at the top of  
111 the column and with a zero pressure head at the bottom. The unknown parameters for the  
112 water flow are the hydraulic parameters:  $k_s$  [ $L.T^{-1}$ ], the saturated hydraulic conductivity;  $\theta_s$   
113 [ $L^3.L^{-3}$ ], the saturated water content;  $\theta_r$  [ $L^3.L^{-3}$ ], the residual water content; and  $\alpha$  [ $L^{-1}$ ] and  
114  $n$  [-], the MvG shape parameters. The only unknown parameter of the tracer transport is the  
115 longitudinal dispersivity,  $a_L$  [L].

116 Several scenarios corresponding to different sets of measurements are investigated to address  
117 the following questions:

118 1) Can we obtain an appropriate estimation of all flow and transport parameters from  
119 tracer-infiltration experiments, even though a limited range in water content is covered

120 (only moderately dry conditions are obtained because of gravity drainage conditions  
121 prescribed at the bottom of the soil column)?

122 2) What is the optimal set of measurements for the estimation of all the parameters? Can  
123 we use only non-intrusive measurements (cumulative outflow and concentration  
124 breakthrough curve) or are intrusive measurements of pressure heads and/or water  
125 contents inside the column unavoidable?

126 3) Is there an optimal design for the tracer injection?

127 For this purpose, synthetic scenarios are considered in the sequel in which data from  
128 numerical simulations are used to avoid the uncontrolled noise of experiments that could bias  
129 the conclusions.

130 The paper is organized as follows. The mathematical models describing flow and transport in  
131 the unsaturated zone are detailed in section 2. Section 3 describes the MCMC Bayesian  
132 parameter estimation procedure used in the DREAM<sub>(ZS)</sub> sampler. Section 4 presents the  
133 different investigated scenarios and discusses the results of the calibration in terms of mean  
134 parameter values and uncertainty ranges for each scenario. Conclusions are given in section 5.  
135

## 136 **2. Unsaturated flow-transport model**

137 We consider a uniform soil profile in the column and an injection of a solute tracer such as  
138 bromide, as described in Mertens et al. (2009). The unsaturated water flow in the vertical soil  
139 column is modeled with the one-dimensional pressure head form of the RE:

$$140 \left\{ \begin{array}{l} \left( c(h) + S_s \frac{\theta}{\theta_s} \right) \frac{\partial h}{\partial t} = \frac{\partial q}{\partial z} \\ q = K(h) \left( \frac{\partial h}{\partial z} - 1 \right) \end{array} \right. , \quad (1)$$

141 where  $h$  [L] is the pressure head;  $q$  [ $L.T^{-1}$ ] is the Darcy velocity;  $z$  [L] is the depth, measured  
 142 as positive in the downward direction;  $S_s$  (-) is the specific storage;  $\theta$  and  $\theta_s$  [ $L^3.L^{-3}$ ] are the  
 143 actual and saturated water contents, respectively;  $c(h)$  [ $L^{-1}$ ] is the specific moisture capacity;  
 144 and  $K(h)$ [ $L.T^{-1}$ ] is the hydraulic conductivity. The latter two parameters are both functions  
 145 of the pressure head. In this study, the relations between the pressure head, conductivity and  
 146 water content are described by the following standard models of Mualem (1976) and van  
 147 Genuchten (1980):

$$148 \quad S_e(h) = \frac{\theta(h) - \theta_r}{\theta_s - \theta_r} = \begin{cases} \frac{1}{(1 + |\alpha h|^n)^m} & h < 0 \\ 1 & h \geq 0 \end{cases} \quad (2)$$

$$K(S_e) = K_s S_e^{1/2} \left[ 1 - (1 - S_e^{1/m})^m \right]^2$$

149 where  $S_e$  (-) is the effective saturation,  $\theta_r$  [ $L^3.L^{-3}$ ] is the residual water content,  $K_s$  [ $L.T^{-1}$ ] is  
 150 the saturated hydraulic conductivity, and  $m=1-1/n$ ,  $\alpha$  [ $L^{-1}$ ] and  $n$  (-) are the MvG shape  
 151 parameters.

152 The tracer transport is governed by the following convection-dispersion equation:

$$153 \quad \frac{\partial(\theta C)}{\partial t} + \frac{\partial(qC)}{\partial z} - \frac{\partial}{\partial z} \left( \theta D \frac{\partial C}{\partial z} \right) = 0 \quad (3)$$

154 where  $C$  [ $M.L^{-3}$ ] is the concentration of the tracer,  $D$  [ $L^2.T^{-1}$ ] is the dispersion coefficient in  
 155 which  $D = a_l q + d_m$  and  $a_l$  [L] is the dispersivity coefficient of the soil and  $d_m$  [ $L^2.T^{-1}$ ] is  
 156 the molecular diffusion coefficient, which is set as  $1.04 \cdot 10^{-4} \text{ cm}^2/\text{min}$ .

157 The transport equation (3) is coupled with the flow equation (1) by the water content  $\theta$  and  
 158 the Darcy's velocity  $q$ . The initial conditions are as follows: a hydrostatic pressure  
 159 distribution with zero pressure head at the bottom of the column ( $z=L$ ) and a solute  
 160 concentration of zero inside the whole column. An infiltration with a flux  $q_{inj}$  of contaminated

161 water with a concentration  $C_{inj}$  is then applied at the upper boundary condition ( $z = 0$ ) during  
 162 a period  $T_{inj}$ . Hence, the boundary conditions at the top of the column can be expressed as:

163

164

$$165 \quad \text{for } 0 < t \leq T_{inj} \left\{ \begin{array}{l} K \left( \frac{\partial h}{\partial z} - 1 \right) = q_{inj} \\ \theta D \frac{\partial C}{\partial z} + qC = q_{inj} C_{inj} \end{array} \right. \quad \text{for } t > T_{inj} \left\{ \begin{array}{l} K \left( \frac{\partial h}{\partial z} - 1 \right) = 0 \\ C_{inj} = 0 \end{array} \right. , \quad (4)$$

166

167 A zero pressure head is maintained at the lower boundary ( $z = L$ ) of the column and a zero  
 168 concentration gradient is used as the lower boundary condition for the solute transport,  
 169 namely,

$$170 \quad (h)_{z=L} = 0 \quad \left( \frac{\partial C}{\partial z} \right)_{z=L} = 0 \quad (5)$$

171 In the sequel, the infiltration rate and the injected solute concentration are  $q_{inj} = 0.015$  cm/min  
 172 and  $C_{inj} = 1$  g/cm<sup>3</sup>, respectively. The system (1)-(5) is solved using the standard finite  
 173 difference method for both flow and transport spatial discretization. A uniform mesh of 600  
 174 cells is employed. Temporal discretization is performed with the high-order method of lines  
 175 (MOL) (e.g., Miller et al., 1998; Tocci et al., 1997; Younes et al., 2009; Fahs et al., 20011).  
 176 Error checking, robustness, order selection and adaptive time step features, available in  
 177 sophisticated solvers, are applied to the time integration of partial differential equations  
 178 (Tocci et al., 1997). The MOL has been successfully used to solve RE in many studies (e.g.,  
 179 Farthing et al., 2003; Miller et al., 2006; Li et al., 2007; Fahs et al., 2009). Details on the use  
 180 of the MOL for solving RE are described in Fahs et al. (2009).



### 181 3. Bayesian parameter estimation

182 The vector of unknown parameters that has to be identified by model calibration is  
183  $\xi = (k_s, \theta_s, \theta_r, \alpha, n, a_L)$ . To analyze the performance of the model calibration procedures, a  
184 reference solution is generated by simulating the flow-transport problem (1)-(5) using the  
185 following parameter values (corresponding to a sandy clay loam soil):  $k_s = 50 \text{ cm/day}$ ,  
186  $\theta_s = 0.43$ ,  $\theta_r = 0.09$ ,  $\alpha = 0.04 \text{ cm}^{-1}$ ,  $n = 1.4$  and  $a_L = 0.2 \text{ cm}$ . Four types of variables are  
187 extracted from the results of the simulation: the pressure head and water content 5 cm below  
188 the top of the column, the cumulative outflow and the solute breakthrough concentration at  
189 the outflow of the column. These four data series are modified by adding a normally  
190 distributed white noise using the following standard deviations:  $\sigma_h = 1 \text{ cm}$  for the pressure  
191 head,  $\sigma_\theta = 0.02$  for the water content,  $\sigma_Q = 0.1 \text{ cm}$  for the cumulative outflow and  $\sigma_c = 0.01$   
192  $\text{g/cm}^3$  for the exit concentration. These perturbations mimic measurement errors and the  
193 resulting values of water pressure, water content, cumulative outflow and solute breakthrough  
194 concentration are considered as measurements in the following.

195 The flow-transport model is used to analyze the effects of different measurement sets on  
196 parameter identification. For this purpose, we adopt a Bayesian approach that involves the  
197 parameter joint posterior distribution (Vrugt et al., 2008). The latter is assessed with the  
198 DREAM<sub>(ZS)</sub> MCMC sampler (Laloy and Vrugt, 2012). This software generates random  
199 sequences of parameter sets that asymptotically converge toward the target joint posterior  
200 distribution (Gelman et al., 1997). Thus, if the number of runs is sufficiently high, the  
201 generated samples can be used to estimate the statistical measures of the posterior  
202 distribution, such as the mean and variance among other measures.

203 The Bayes theorem states that the probability density function of the model parameters  
204 conditioned onto data can be expressed as:

205 
$$p(\xi | \mathbf{y}_{mes}) \propto p(\mathbf{y}_{mes} | \xi) p(\xi), \quad (6)$$

206 where  $p(\xi | \mathbf{y}_{mes})$  is the likelihood function measuring how well the model fits the  
 207 observations  $\mathbf{y}_{mes}$ , and  $p(\xi)$  is the prior information about the parameter before the  
 208 observations are made. Independent uniform priors within the ranges reported in Table 1 are  
 209 chosen. In this work, a Gaussian distribution defines the likelihood function because the  
 210 *observations* are simulated and corrupted with Gaussian errors. Hence, the parameter  
 211 posterior distribution is expressed as:

212 
$$p(\xi / \mathbf{y}_{mes}) \propto \exp\left(-\frac{SS_h(\xi)}{2\sigma_h^2} - \frac{SS_\theta(\xi)}{2\sigma_\theta^2} - \frac{SS_Q(\xi)}{2\sigma_Q^2} - \frac{SS_C(\xi)}{2\sigma_C^2}\right), \quad (7)$$

213 where  $SS_h(\xi)$ ,  $SS_\theta(\xi)$ ,  $SS_Q(\xi)$  and  $SS_C(\xi)$  are the sums of the squared differences  
 214 between the observed and modeled data of the pressure head, water content, cumulative  
 215 outflow and output concentration, respectively. For instance,  $SS_h(\xi) = \sum_{k=1}^{Nh} (h_{mes}^{(k)} - h_{mod}^{(k)}(\xi))^2$ ,  
 216 which includes the observed  $h_{mes}^{(k)}$  and predicted  $h_{mod}^{(k)}$  pressure heads at time  $t_k$  for the number  
 217 of pressure head observations  $Nh$ .

218 Bayesian parameter estimation is performed hereafter with the DREAM<sub>(ZS)</sub> software (Laloy  
 219 and Vrugt, 2012), which is an efficient MCMC sampler. DREAM<sub>(ZS)</sub> computes multiple sub-  
 220 chains in parallel to thoroughly explore the parameter space. Archives of the states of the sub-  
 221 chains are stored and used to allow a strong reduction of the "burn-in" period in which the  
 222 sampler generates individuals with poor performances. Taking the last 25% of individuals of  
 223 the MCMC (when the chains have converged) yields multiple sets of parameters,  $\xi$ , that  
 224 adequately fit the model onto observations. These sets are then used to estimate the updated  
 225 parameter distributions, the pairwise parameter correlations and the uncertainty of the model

226 predictions. As suggested in Vrugt et al. (2003b), we consider that the posterior distribution is  
227 stationary if the Gelman and Ruban (1992) criterion is  $\leq 1.2$ .

## 228 **4. Results and discussion**

229 In this section, the identifiability of the parameters is investigated for 7 different scenarios of  
230 measurement sets (Table 1). In the first scenario, only measured pressure heads and  
231 cumulative outflow are used for the calibration. The scenarios 2 to 5 investigate the benefit of  
232 adding measured water contents and/or solute outlet concentrations to pressure heads and  
233 outflow. The last scenarios (6, 7) investigate the use of measured cumulative outflow and  
234 concentration breakthrough at the column outflow because these measurements do not require  
235 intrusive techniques. Scenarios 5 to 7 investigate as well the effects of solute injection  
236 duration on the identifiability of the parameters.

237

238 In all cases, the MCMC sampler was run with 3 simultaneous chains for a total number of  
239 50000 runs. Depending on the scenario, the MCMC required between 5000 and 20000 model  
240 runs to reach convergence and was terminated after 30000 runs. The last 25% of the runs that  
241 adequately fit the model onto observations are used to estimate the updated probability  
242 density function (pdf).

243

### 244 ***4.1. The data sets for parameter estimation***

245 The data sets obtained from solving the flow-transport problems (1)-(5) using the parameters  
246 given in section 2 are shown in Fig. 1. The pressure head at 5 cm from the top of the column  
247 (Fig. 1a) increases from its initial hydrostatic negative value (-115 cm) and reaches a plateau  
248 (-1.75 cm) in less than 100 minutes during the injection period. After the injection is finished,  
249 it progressively decreases due to the drainage caused by the gravity effect. A similar behavior  
250 is observed for the water content at the same location (Fig. 1b), where the value of the plateau

251 is close to the saturation value. The cumulative outflow (Fig. 1c) starts to increase at  
252 approximately 1000 min after the beginning of the injection. It shows an almost linear  
253 behavior until 5500 min. It then slowly increases with an asymptotic behavior due to the  
254 natural drainage after the end of the injection period. Fig. 1d displays the water saturation as a  
255 function of the pressure head. It is worth noting that only a few part of this curve is described  
256 during the infiltration experiment. Indeed, only moderate dry conditions are established  
257 because the minimum pressure head reached in the column is -120 cm, which corresponds to  
258 the initial pressure head at the top of the column.

259 The breakthrough concentration curve (Fig. 1e) shows a sharp front, which starts shortly after  
260 3000 min. Note that if the injection of both water and contaminant are stopped once the solute  
261 reaches the output. For an injection period of 3000 min, the breakthrough curve exhibits a  
262 smoother progression (Fig. 1f).

263 The data considered as measurements, which are used as conditioning information for model  
264 calibration, are also shown in Fig. 1. In Fig. 1b, the water content seems to be more affected  
265 by the perturbation of data than the pressure head and cumulative outflow. This phenomenon  
266 is due to the relative importance of the measurement errors of the water content often  
267 observed with time-domain-reflectometry probes and to the weak variations of the water  
268 content during the infiltration experiment. The perturbation of the breakthrough curve is  
269 relatively small because of the low added noise since output concentrations can be accurately  
270 measured. The perturbations of the pressure head and cumulative outflow seem weak because  
271 of the large variation of these variables during the experiment.

272

#### 273 ***4.2. Results of the parameter estimation***

274 The uncertainty model parameters are assumed to be distributed uniformly over the ranges  
275 reported in Table 1. This table also lists the reference values used to generate data

276 observations before perturbation. Seven scenarios are considered, corresponding to different  
277 sets of measurements for the estimation of the hydraulic and transport soil parameters (Table  
278 2).

279 The MCMC results of the seven studied scenarios are given in Figs. 2 to 8. The "on-diagonal"  
280 plots in these figures display the inferred parameter distributions, whereas the "off-diagonal"  
281 plots represent the pairwise correlations in the MCMC sample. If the draws are independent,  
282 non-sloping scatterplots should be observed. However, if a good value of a given parameter is  
283 conditioned by the value of another parameter, then their pairwise scatterplot should show a  
284 narrow sloping stripe. The sensitivity of parameters is obtained by comparing prior to  
285 posterior parameter distribution. A significant difference between the two distributions for a  
286 parameter indicates high model sensitivity to that parameter (Dusek et al., 2015).

287 To facilitate the comparison between the different scenarios, Figs. 9 to 14 show the mean and  
288 the 95% confidence intervals of the final MCMC sample that adequately fit the model onto  
289 observations for each scenario, and Table 3 summarizes the pairwise parameter correlations.

290 Fig. 2 shows the inferred distributions of the parameters identified with the MCMC sampler  
291 using only the pressure and cumulative outflow measurements (scenario 1). The parameters  
292  $k_s$ ,  $\alpha$  and  $n$  are well estimated; their prior intervals of variation are strongly narrowed and  
293 they essentially show bell-shaped posterior distributions. This shows the high sensitivity of  
294 the model responses to these parameters.

295 The parameter  $k_s$  is strongly correlated to  $\alpha$  (0.94) and  $n$  (-0.97). These results confirmed  
296 the results of Eching and Hopmans (1994) on multistep outflow experiments who found that  
297 the inverse solution technique is greatly improved when both cumulative outflow and pressure  
298 head data from some positions inside the column are used. The two water contents related  
299 parameters are strongly correlated (0.96) and cannot be identified accurately because the  
300 water retention relationship depends on the difference between  $\theta_s$  and  $\theta_r$  and only this

301 difference is identifiable. Note that the prior intervals of  $\theta_r$  and  $\theta_s$  which are respectively  
302  $[0.05, 0.2]$  and  $[0.3, 0.5]$  have changed to the posterior intervals  $[0.05, 0.16]$  and  $[0.39, 0.5]$   
303 because the target difference should be  $\theta_s - \theta_r = 0.34$ . In the literature, van Genuchten and  
304 Nielsen (1985), Eching and Hopmans (1993) and Zurmühl (1996) considered that saturated  
305 water content is determined independently and considered only  $\theta_r$  to be an empirical  
306 parameter that should be fitted to the data.

307 The dispersivity coefficient  $a_l$  has not been identified in this first scenario.

308 The MCMC results in Fig. 3 show that water content measurements throughout the  
309 experiment (scenario 2) allow the estimation of both the residual and saturated water contents.

310 The parameter  $\theta_r$  strongly correlates to  $k_s$  (-0.94) and  $n$  (0.98) and the parameter  $k_s$  remains  
311 strongly related to  $\alpha$  (0.94) and  $n$  (-0.98). Although the water content data are subject to  
312 relatively high measurement errors, a good estimation is obtained for  $\theta_s$  and  $\theta_r$ . The  
313 parameters  $k_s$ ,  $\alpha$  and  $n$  are estimated with the same accuracy as for the first scenario. All  
314 parameters (except the dispersivity coefficient) are highly sensitive since their posterior  
315 intervals of variations are strongly reduced compared to the prior intervals. Moreover, the  
316 prior uniform distributions give place to almost Gaussian posterior distributions. These results  
317 show that, although Kool et al. (1985) and Kool and Parker (1988) suggested that the transient  
318 experiments should cover a wide range in water content, an appropriate estimation of all  
319 parameters can be obtained with the infiltration experiment even though a limited range in  
320 water content is covered.

321 When the concentration measurements are also considered in the inversion (scenario 3), the  
322 results depicted in Fig. 4 show very significant correlations between  $k_s$  and  $\theta_r$  (-0.94),  $k_s$   
323 and  $\alpha$  (0.91),  $k_s$  and  $n$  (-0.97) and  $n$  and  $\theta_r$  (0.99). The posterior uncertainty ranges of  $k_s$ ,

324  $\alpha$ ,  $n$  and  $\theta_r$  are similar to the previous scenarios. Those of  $\theta_s$  and  $a_l$  are strongly reduced,  
325 leading to a good identification of these parameters when using  $C$  measurements (Figs. 10  
326 and 14). A better estimate of the saturated water content is obtained because advective  
327 transport is a function of this variable.

328 In the inversion procedure of scenario 4, the measurements of the water content are not  
329 considered. This scenario leads to the same quality of the estimation for the parameters  $k_s$ ,  $\theta_r$ ,  
330  $\alpha$  and  $n$  (Figs. 9, 11, 12, 13) and similar correlations between the parameters as in the  
331 previous scenario. This result shows that the intrusive water content measurements, which are  
332 subject to more significant measurement errors than the output concentration, are not required  
333 if the output concentration is measured. Compared with the results of scenario 2, it can be  
334 concluded that better parameter estimations are obtained using  $h$ ,  $Q$  and  $C$  data than using  
335  $h$ ,  $Q$  and  $\theta$  data, especially for  $\theta_s$ . Therefore, using  $C$  instead of  $\theta$  measurements in  
336 combination with  $h$  and  $Q$  measurements allows the estimation of  $a_l$  and yields better  
337 estimate of  $\theta_s$ .

338 The pressure head, cumulative outflow and concentration measurements are used in the  
339 estimation procedure of scenario 5, but the injection period is now reduced to  $T_{inj} = 3000 \text{ min}$ .  
340 The obtained results (Fig. 6) show the same correlations between the parameters as for  
341  $T_{inj} = 5000 \text{ min}$ . For the parameters  $k_s$ ,  $\theta_s$ ,  $\theta_r$ ,  $\alpha$  and  $n$ , almost the same mean estimates are  
342 obtained as for scenario 4. However, the parameters are better identified (Figs. 9 to 13).  
343 Indeed, the uncertainty of these parameters is smaller because the credible interval is reduced  
344 by a factor of 25% for  $k_s$ , 8% for  $\theta_s$ , 26% for  $\theta_r$ , 10% for  $\alpha$  and 25% for  $n$  when compared  
345 to the results obtained using  $T_{inj} = 5000 \text{ min}$ . The parameter  $a_l$  is also much better estimated  
346 than in the previous scenario. Its mean value approaches the reference solution and the  
347 posterior uncertainty range is reduced by approximately 75% (Fig. 14).

348 In scenario 6, the pressure head measurements are removed and only non-intrusive  
 349 measurements ( $Q$  and  $C$  data) are used for the calibration with an injection period of  
 350  $T_{inj} = 5000\text{min}$ . These kind of nonintrusive measures have been used by Mertens et al. (2009)  
 351 to estimate some of hydraulic and pesticides leaching parameters. The results depicted in Fig.  
 352 7 show high correlations only between  $k_s$  and  $n$  (-0.95) and  $\theta_r$  and  $n$  (0.95). On the one  
 353 hand, these results show that all the parameters are well estimated since, as compared to the  
 354 prior intervals (given in Table 1), the confidence intervals of the estimated parameters (plotted  
 355 in Figs. 9-14) are strongly reduced, especially for the parameters  $\alpha$ ,  $n$  and  $\theta_s$ . On the other  
 356 hand, compared to the results of scenario 4 which also considers pressure data,  $k_s$  is not as  
 357 well estimated (the mean value is less close to the reference value and the confidence interval  
 358 is 27% larger). The mean estimated values for  $\theta_r$  and  $n$  also degraded (less close to the  
 359 reference solution), although their confidence intervals are similar to those of scenario 4  
 360 (Figs. 11, 13). The estimated mean value of the parameter  $\alpha$  is similar to that in scenario 4.  
 361 However, its uncertainty is much larger because the credible interval is 77% larger (Fig. 14).  
 362 The parameters  $\theta_s$  and  $a_l$  are estimated as well as in scenario 4 (in terms of mean estimated  
 363 value and credible interval).  
 364 The last scenario (scenario 7) is similar to the previous one, but the injection period is reduced  
 365 to  $T_{inj} = 3000\text{min}$ . The results depicted in Fig. 8 show similar correlations between the  
 366 parameters as for  $T_{inj} = 5000\text{min}$ . However, a significant improvement is observed for the  
 367 mean estimated values, which approach the reference solution for  $k_s$ ,  $\theta_r$ ,  $n$  and  $a_l$  (Figs. 9,  
 368 11, 13, 14). The uncertainties of  $k_s$ ,  $\alpha$  and  $a_l$  are also reduced by approximately 40%, 15%  
 369 and 70%, respectively. The parameter  $\theta_s$  is estimated as well as in scenario 6. The  
 370 improvement of the parameter estimation in this last scenario compared to the previous one



371 can be explained by the fact that the injection of water and solute contaminant is stopped once  
372 the concentration reaches the column outlet. Hence, the injected volume ( $0.015 \times 3000 =$   
373  $45 \text{ cm}^3/\text{cm}^2$ ) is slightly less than the pore volume ( $120 \times 0.43 = 51 \text{ cm}^3/\text{cm}^2$ ). Thus, when the  
374 injection is stopped, the column is not fully saturated and the outlet flux strongly reduces (see  
375 the asymptotic behavior of the cumulative outflow when the injection is stopped in Fig. 1c).  
376 As a consequence, the concentration profile increases smoothly (see Fig. 1f) until reaching its  
377 maximum value in contrast to the sharp front observed for  $T_{inj} = 5000 \text{ min}$  in the scenario 6  
378 (see Fig. 1e). Hence, the breakthrough curve obtained with  $T_{inj} = 3000 \text{ min}$  is more affected  
379 by the hydraulic parameters than the breakthrough curve obtained with  $T_{inj} = 5000 \text{ min}$ . This  
380 explains why a better estimation of the parameters is observed for the last scenario compared  
381 to the scenario 6.

382

## 383 5. Conclusions

384 In this work, estimation of hydraulic and transport soil parameters have been investigated  
385 using synthetic infiltration experiments performed in a column filled with a sandy clay loam  
386 soil, which was subjected to continuous flow and solute injection over a period  $T_{inj}$ .

387 The saturated hydraulic conductivity, the saturated and residual water contents, the Mualem-  
388 van Genuchten shape parameters and the longitudinal dispersivity are estimated in a Bayesian  
389 framework using the Markov Chain Monte Carlo (MCMC) sampler. Parameter estimation is  
390 performed for different scenarios of data measurements.

391 The results reveal the following conclusions:

- 392 1. All hydraulic and transport parameters can be appropriately estimated from the  
393 described infiltration experiment. However, the accuracy differs and depends on the

394 type of measurement and the duration of the injection  $T_{inj}$ , even if the water content  
395 remains close to saturated conditions.

396 2. The use of concentration measurements at the column outflow, in addition to  
397 traditional measured variables (water content, pressure head and cumulative outflow),  
398 reduces the hydraulic parameters uncertainties, especially that of the saturated water  
399 content (comparison between scenario 2 and scenario 3).

400 3. The saturated hydraulic conductivity is estimated with the same order of accuracy,  
401 independent of the observed variables.

402 4. The estimation of the dispersivity is sensitive to the injection duration. The scenarios 5  
403 and 7 with  $T_{inj} = 3000\text{min}$  yield much more accurate dispersivity estimations than  
404 scenarios 4 and 6 with  $T_{inj} = 5000\text{min}$  due to the extended spreading of the solute  
405 observed for  $T_{inj} = 3000\text{min}$ .

406 5. A better identifiability of the soil parameters is obtained using  $C$  instead of  $\theta$   
407 measurements, in combination with  $h$  and  $Q$  data (comparison between scenario 2  
408 and scenario 4).

409 6. Using only non-intrusive measurements (cumulative outflow and output  
410 concentration) yields satisfactory estimation of all parameters (scenario 7). The  
411 uncertainty of the parameters significantly decreases when the injection of water and  
412 solute is maintained for a limited period (comparison between scenario 6 and scenario  
413 7).

414

415 This last point has practical applications for designing simple experimental setups dedicated  
416 to the estimation of hydrodynamic and transport parameters for unsaturated flow in soils. The  
417 setup has to be appropriately equipped to measure the cumulative water outflow (e.g.,

418 weighing machine) and the solute breakthrough at the column outflow (e.g., flow through  
419 electrical conductivity). The injection should be stopped as soon as the solute concentration  
420 reaches the outflow. The accuracy of the estimation of  $\theta_r$ ,  $\alpha$  and  $n$  improves by adding  
421 pressure measurements inside the column, close to the injection.

422

423 These results are of course related to the models and experimental conditions we used. This  
424 work can be extended to different types of soils, water retention and/or relative permeability  
425 functions to evaluate the interest of coupling flow and transport for parameter identification.  
426 This work can also be extended to reactive solutes.

427

428

#### 429 **Acknowledgments**

430 The authors are grateful to the French National Research Agency, which funded this work  
431 through the program AAP Blanc - SIMI 6 project RESAIN (n°ANR-12-BS06-0010-02).

432

433  
434  
435  
436  
437  
438  
439  
440  
441  
442  
443  
444  
445  
446  
447  
448  
449  
450  
451  
452  
453  
454  
455  
456  
457  
458  
459  
460  
461  
462  
463  
464  
465  
466

**References**

Ades A.E., G. Lu. 2003. Correlations between parameters in risk models: estimation and propagation of uncertainty by Markov Chain Monte Carlo. *Risk Anal.* 23(6):1165-72.

Carrera J., and S.P. Neuman. 1986. Estimation of aquifer parameters under transient and steady conditions: 2. Uniqueness, stability and solution algorithms. *Water Resour. Res.*, 22, 211–227.

Durner W., B. Schultze, T. Zurmühl. 1999. State-of-the-art in inverse modeling of inflow/outflow experiments. p661-681. In M.Th. van Genuchten et al. (ed.) *Characterization and Measurement of the Hydraulic Properties of Unsaturated Porous Media*, Proc. Int. Worksh. Riverside, CA. Univ. of California, Riverside.

Durner W., S.C. Iden. 2011. Extended multistep outflow method for the accurate determination of soil hydraulic properties near water saturation. *Water Resour. Res.* 47:W08526. doi: 10.1029/2011WR010632

Dusek J, M. Dohnal, M. Snehota, M. Sobotkova, C. Ray, T. Vogel. 2015. Transport of bromide and pesticides through an undisturbed soil column: a modeling study with global optimization analysis. *J Contam Hydrol.* Apr-May;175-176:1-16. doi: 10.1016/j.jconhyd.2015.02.002.

Eching S.O., J.W. Hopmans. 1993. Optimization of hydraulic functions from transient outflow and soil water pressure data. *Soil Sci. Soc. Am. J.* 57:1167-1175. doi:10.2136/sssaj1993.03615995005700050001x

Eching S.O., J.W. Hopmans, O. Wendroth. 1994. Unsaturated Hydraulic Conductivity from Transient Multistep Outflow and Soil Water Pressure Data. *Soil Sci. Soc. Am. J.* 58: 687-95 doi:10.2136/sssaj1994.03615995005800030008x

Fahs M., A. Younes, F. Lehmann. 2009. An easy and efficient combination of the Mixed Finite Element Method and the Method of Lines for the resolution of Richards’

467 Equation. *Environmental Modelling & Software* ;24:1122–1126.  
468 doi:10.1016/j.envsoft.2009.02.010  
469  
470 Fahs M., A. Younes, P. Ackerer. 2011. An efficient implementation of the method of lines for  
471 multicomponent reactive transport equations. *Water air and soil pollution*,  
472 vol. 215, no1-4, pp. 273-283. doi:10.1007/s11270-010-0477-y  
473  
474 Farthing M.W., C.E. Kees, C.T. Miller. 2003. Mixed finite element methods and higher order  
475 temporal approximations for variably saturated groundwater flow. *Adv. in Water*  
476 *Resour.* 26:373-394. doi: 10.1016/S0309-1708(02)00187-2  
477  
478 Gallagher M., J. Doherty. 2007. Parameter estimation and uncertainty analysis for a  
479 watershed model. *Environmental Modelling & Software* 22, 1000-1020.  
480 doi:10.1016/j.envsoft.2006.06.007  
481  
482 Gelman A., J.B. Carlin, H.S. Stren, D.B. Rubin. 1997. *Bayesian data analysis*, Chapman and  
483 Hall, London.  
484  
485 Gelman A., D.B. Rubin. 1992. Inference from iterative simulation using multiple sequences.  
486 *Stat. Sci.* 7:457-472.  
487  
488 Hopmans J.W., J. Šimunek, N. Romano, W. Durner. 2002. Simultaneous determination of  
489 water transmission and retention properties. *Inverse Methods*. p963-1008. In J.H. Dane  
490 and G.C. Topp (ed.) *Methods of Soil Analysis. Part 4. Physical Methods*. Soil Science  
491 Society of America Book Series No. 5.  
492  
493 Hudson D.B., P.J. Wierenga, R.G. Hills 1996. Unsaturated hydraulic properties from upward  
494 flow into soil cores. *Soil Sci Soc Am J*;60:388±96.  
495  
496 Inoue M., J. Šimunek J.W. Hopmans, and V. Clausnitzer. 1998. In situ estimation of soil  
497 hydraulic functions using a multistep soil-water extraction technique. *Water Resour.*  
498 *Res.* 34:1035–1050.  
499

500 Inoue M., J. Šimůnek, S. Shiozawa, J.W. Hopmans. 2000. Simultaneous estimation of soil  
501 hydraulic and solute transport parameters from transient infiltration experiments, *Adv.*  
502 *in Water Resour.* 23 (7). Doi : 10.1016/S0309-1708(00)00011-7.  
503

504 Kahl G.M., Y. Sidorenko, B. Gottesbüren. 2015. Local and global inverse modelling  
505 strategies to estimate parameters for pesticide leaching from lysimeter studies. *Pest*  
506 *Manag Sci.* Apr;71(4):616-31. doi: 10.1002/ps.3914.  
507

508 Kool J.B., J.C. Parker, M.Th van Genuchten. 1985. Determining soil hydraulic properties  
509 from one-step outflow experiments by parameter estimation: I. Theory and numerical  
510 studies. *Soil Sci Soc Am J*;49:1348±54.  
511

512 Kool J.B., and J.C. Parker. 1988. Analysis of the inverse problem for transient unsaturated  
513 flow. *Water Resour. Res.* 24:817–830.  
514

515 Laloy E., J.A. Vrugt. 2012. High-dimensional posterior exploration of hydrologic models  
516 using multiple-try DREAM(ZS) and high-performance computing, *Water Resour. Res.*,  
517 48, W01526. doi:10.1029/2011WR010608  
518

519 Li H., M.W. Farthing, C.N. Dawson, C.T. Miller. 2007. Local discontinuous Galerkin  
520 approximations to Richards' equation. *Adv. in Water Resour.* 30:555–575. doi:  
521 10.1016/j.advwatres.2006.04.011  
522

523 Marquardt DW. 1963. An algorithm for least-squares estimation of nonlinear parameters.  
524 *SIAM J Appl Math*;11:431±41.  
525

526 Mertens J., G. Kahl, B. Gottesbüren, J. Vanderborght. 2009. Inverse Modeling of Pesticide  
527 Leaching in Lysimeters: Local versus Global and Sequential Single-Objective versus  
528 Multiobjective Approaches *Vadose Zone J.* 8(3). doi: 10.2136/vzj2008.0029  
529

530 Miller C.T., G.A. Williams, C.T. Kelly, M.D. Tocci. 1998. Robust solution of Richards'  
531 equation for non uniform porous media. *Water Resour. Res.* 34:2599–2610. doi:  
532 10.1029/98WR01673  
533

534 Miller C.T., C. Abhishek, M. Farthing. 2006. A spatially and temporally adaptive solution of  
535 Richards' equation. *Adv. in Water Resour.* 29:525–545. doi:  
536 10.1016/j.advwatres.2005.06.008  
537

538 Mishra S., J.C. Parker. 1989. Parameter estimation for coupled unsaturated flow and  
539 transport. *Water Resour Res.* 25(3). doi: 10.1029/WR025i003p00385  
540

541 Mualem Y. 1976. A new model for predicting the hydraulic conductivity of unsaturated  
542 porous media. *Water Resour. Res.* 12:513–522. doi:10.1029/WR012i003p00513  
543

544 Nasta P., S. Huynh, J.W. Hopmans. 2011. Simplified Multistep Outflow Method to Estimate  
545 Unsaturated Hydraulic Functions for Coarse-Textured Soil *Sci. Soc. Am. J.* 75, p.418.  
546 doi:10.2136/sssaj2010.011  
547

548 Šimůnek, J., and M.Th. van Genuchten. 1997. Estimating unsaturated soil hydraulic  
549 properties from multiple tension disc infiltrometer data. *Soil Sci.* 162:383–398.  
550

551 Tocci M.D., C.T. Kelly, C.T. Miller. 1997. Accurate and economical solution of the pressure-  
552 head form of Richards' equation by the method of lines. *Adv. in Water Resour.* 20:1–  
553 14. doi: 10.1016/S0309-1708(96)00008-5  
554

555 van Dam J.C., J.N.M. Stricker, P. Droogers. 1992. Inverse method for determining soil  
556 hydraulic functions from one-step outflow experiment. *Soil Sci Soc Am J.* 56:1042±50.  
557

558 van Dam J.C., J.N.M. Stricker, P. Droogers. 1994. Inverse method to determine soil hydraulic  
559 functions from multistep outflow experiments. *Soil Sci. Soc. Am. J.* 58:647-652.  
560 doi:10.2136/sssaj1994.03615995005800030002x  
561

562 van Genuchten M.Th. 1980. A closed form equation for predicting the hydraulic conductivity  
563 of unsaturated soils. *Soil Sci. Soc. Am. J.* 44(5):892-898.  
564 doi:10.2136/sssaj1980.03615995004400050002x  
565

566 Van Genuchten M.Th. and D.R. Nielsen. 1985. On describing and predicting the hydraulic  
567 properties of unsaturated soils. *Annales Geophysicae*, 1985, 3, 615–628.

568  
569 Vrugt J.A., W. Bouten. 2002. Validity of first-order approximations to describe parameter  
570 uncertainty in soil hydrologic models. *Soil. Sci. Soc. Am. J.* 66:1740-1751.  
571 doi:10.2136/sssaj2002.1740  
572  
573 Vrugt J.A., W. Bouten, H.V. Gupta, J.W. Hopmans. 2003a. Toward improved identifiability  
574 of soil hydraulic parameters: On the selection of a suitable parametric model. *Vadose*  
575 *Zone J.* 2:98–113. doi: 10.2113/2.1.98  
576  
577 Vrugt J.A., H.V. Gupta, W. Bouten, S. Sorooshian. 2003b. A shuffled complex evolution  
578 Metropolis algorithm for optimization and uncertainty assessment for hydrologic model  
579 parameters. *Water Resour. Res.* 39(8):1201, doi:10.1029/2002WR001642.  
580  
581 Vrugt J.A., C.J.F. ter Braak, M.P. Clark, J.M. Hyman, B.A. Robinson. 2008. Treatment of  
582 input uncertainty in hydrologic modeling: Doing hydrology backward with Markov  
583 chain Monte Carlo simulation. *Water Resour. Res.*, 44, W00B09. doi:  
584 10.1029/2007WR006720.  
585  
586 Younes A., M. Fahs, S. Ahmed. 2009. Solving density driven flow problems with efficient  
587 spatial discretizations and higher-order time integration methods. *Advances in Water*  
588 *Resources* 2009, 32 (3) pp 340-352, doi:10.1016/j.advwatres.2008.11.003.  
589  
590 Younes A., T.A. Mara, N. Fajraoui, F. Lehmann, B. Belfort, H. Beydoun. 2013. Use of  
591 Global Sensitivity Analysis to Help Assess Unsaturated Soil Hydraulic Parameters.  
592 *Vadose Zone J.* 12. doi:10.2136/vzj2011.0150.  
593  
594 Zurmühl T. 1996. Evaluation of different boundary conditions for independent determination  
595 of hydraulic parameters using outflow methods. In *Parameter Identification and Inverse*  
596 *Problems in Hydrology, Geology and Ecology*, eds. J.Gottlieb and P. DuChateau.  
597 Kluwer, Dordrecht, 1996, pp.165–184.  
598



599

600 **List of table captions**

601

602 Table 1. Prior lower and upper bounds of the uncertainty parameters and reference values.

603

604 Table 2. Measurement sets and injection periods for the different scenarios. The pressure head  
605  $h$  and the water content  $\theta$  are measured at 5 cm from the top of the column. The cumulative  
606 outflow  $Q$  and the concentration  $C$  are measured at the exit of the column.

607

608 Table 3. Summary of the pairwise parameter correlations.

609

610

Parameters	Lower bounds	Upper bounds	Reference values
$k_s$ [cm min <sup>-1</sup> ]	0.025	0.1	0.0347
$\theta_s$ [-]	0.3	0.5	0.43
$\theta_r$ [-]	0.05	0.2	0.09
$\alpha$ [cm <sup>-1</sup> ]	0.01	0.3	0.04
$n$ [-]	1.2	5	1.4
$a_l$ [cm]	0.05	0.6	0.2

611

612 Table 1. Prior lower and upper bounds of the uncertainty parameters and reference values.

613

614

615

616

Scenario	Measured variables				Injection period	
	$h$	$\theta$	$Q$	$C$	$T_{inj} = 5000$ min	$T_{inj} = 3000$ min
<b>1</b>	v		v		v	
<b>2</b>	v	v	v		v	
<b>3</b>	v	v	v	v	v	
<b>4</b>	v		v	v	v	
<b>5</b>	v		v	v		v
<b>6</b>			v	v	v	
<b>7</b>			v	v		v

617

618 Table 2. Measurement sets and injection periods for the different scenarios. The pressure head  
619  $h$  and the water content  $\theta$  are measured at 5 cm from the top of the column. The cumulative  
620 outflow  $Q$  and the concentration  $C$  are measured at the exit of the column.

621

622

623

624

625

626

627

Scenario				
1	$(k_s, n) = -0.97$	$(k_s, \alpha) = 0.94$		$(\theta_r, \theta_s) = 0.96$
2	$(k_s, n) = -0.98$	$(k_s, \alpha) = 0.94$	$(k_s, \theta_r) = -0.94$	$(\theta_r, n) = 0.98$
3	$(k_s, n) = -0.97$	$(k_s, \alpha) = 0.91$	$(k_s, \theta_r) = -0.94$	$(\theta_r, n) = 0.99$
4	$(k_s, n) = -0.98$	$(k_s, \alpha) = 0.95$	$(k_s, \theta_r) = -0.96$	$(\theta_r, n) = 0.99$
5	$(k_s, n) = -0.96$	$(k_s, \alpha) = 0.93$	$(k_s, \theta_r) = -0.91$	$(\theta_r, n) = 0.98$
6	$(k_s, n) = -0.95$			$(\theta_r, n) = 0.95$
7	$(k_s, n) = -0.95$			$(\theta_r, n) = 0.94$

628

Table 3. Summary of the pairwise parameter correlations.

629

630

631  
632  
633  
634  
635  
636  
637  
638  
639  
640  
641  
642  
643  
644  
645  
646  
647  
648  
649  
650  
651  
652  
653  
654  
655  
656  
657  
658

**List of figure captions**

Fig. 1. (a) Pressure head at 5 cm below the soil surface, (b) water content at 5 cm below the soil surface, (c) cumulative outflow, (d) retention curve, (e) output concentration for  $T_{inj} = 5000$  and (f) for  $T_{inj} = 3000$  min. Solid lines represent model outputs and dots represent the sets of perturbed data serving as conditioning information for model calibration.

Fig. 2. MCMC solutions for the transport scenario 1. The diagonal plots represent the inferred posterior probability distribution of the model parameters. The off-diagonal scatterplots represent the pairwise correlations in the MCMC drawing.

Fig. 3. MCMC solutions for transport scenario 2 [see Fig. 2 caption].

Fig. 4. MCMC solutions for transport scenario 3 [see Fig. 2 caption].

Fig. 5. MCMC solutions for transport scenario 4 [see Fig. 2 caption].

Fig. 6. MCMC solutions for transport scenario 5 [see Fig. 2 caption].

Fig. 7. MCMC solutions for transport scenario 6 [see Fig. 2 caption].

Fig. 8. MCMC solutions for transport scenario 7 [see Fig. 2 caption].

Fig. 9. Posterior mean values and 95% confidence intervals of the saturated hydraulic conductivity for the different scenarios.

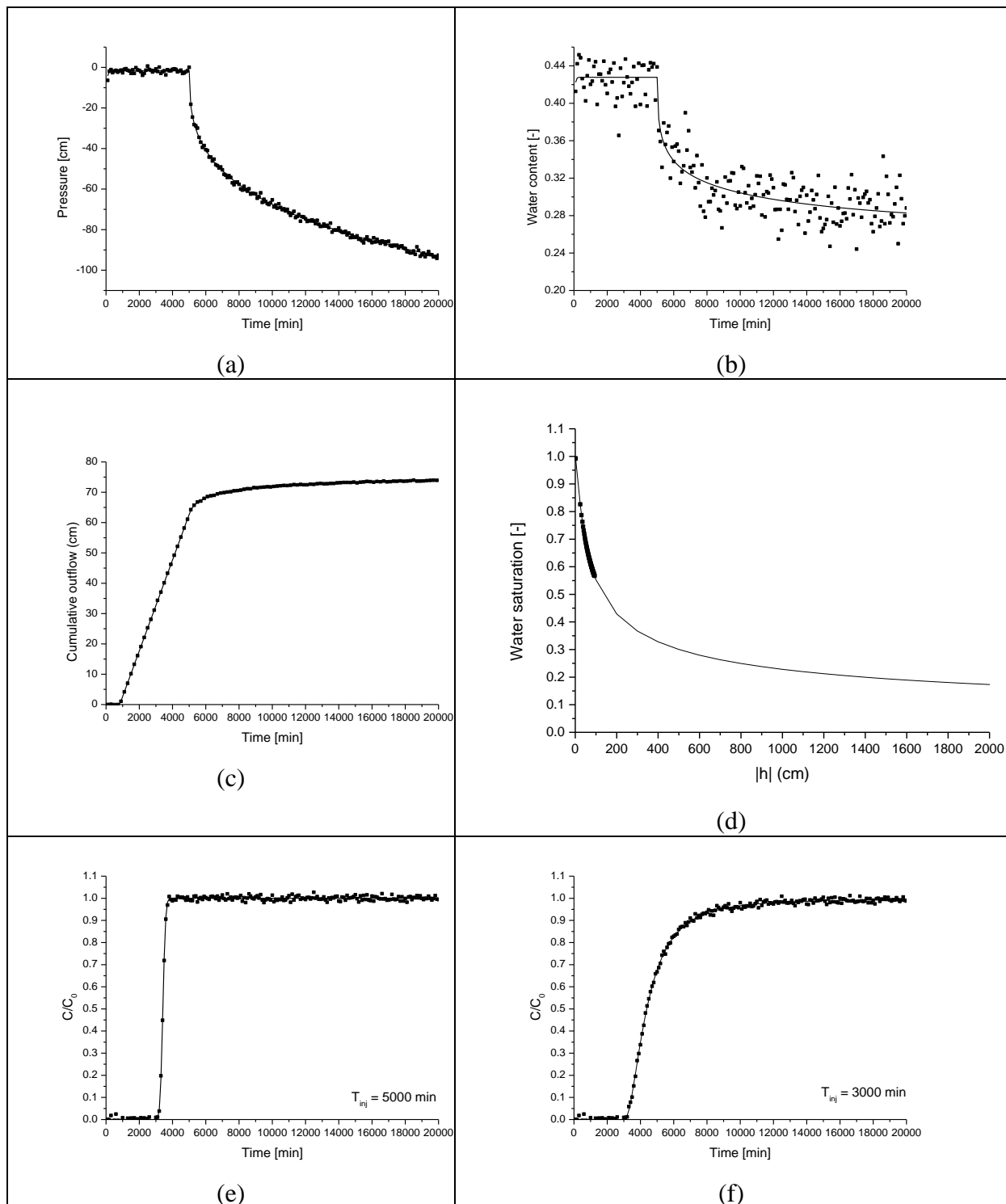
Fig. 10. Posterior mean values and 95% confidence intervals of the saturated water content for the different scenarios.

Fig. 11. Posterior mean values and 95% confidence intervals of the residual water content for the different scenarios.

Fig. 12. Posterior mean values and 95% confidence intervals of the shape parameter  $\alpha$  for the different scenarios.

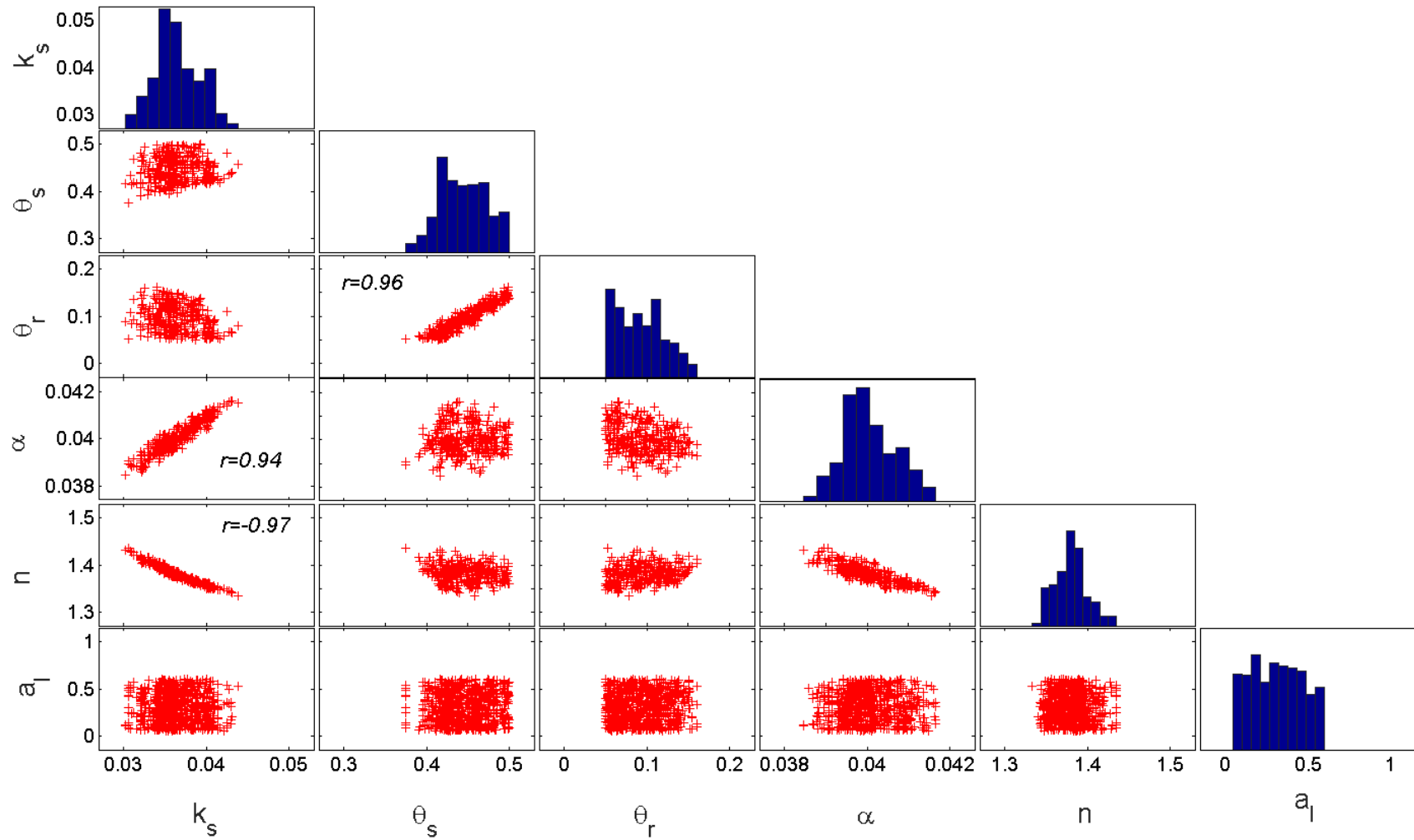
Fig. 13. Posterior mean values and 95% confidence intervals of the shape parameter  $n$  for the different scenarios.

Fig. 14. Posterior mean values and 95% confidence intervals of dispersivity for the different scenarios.

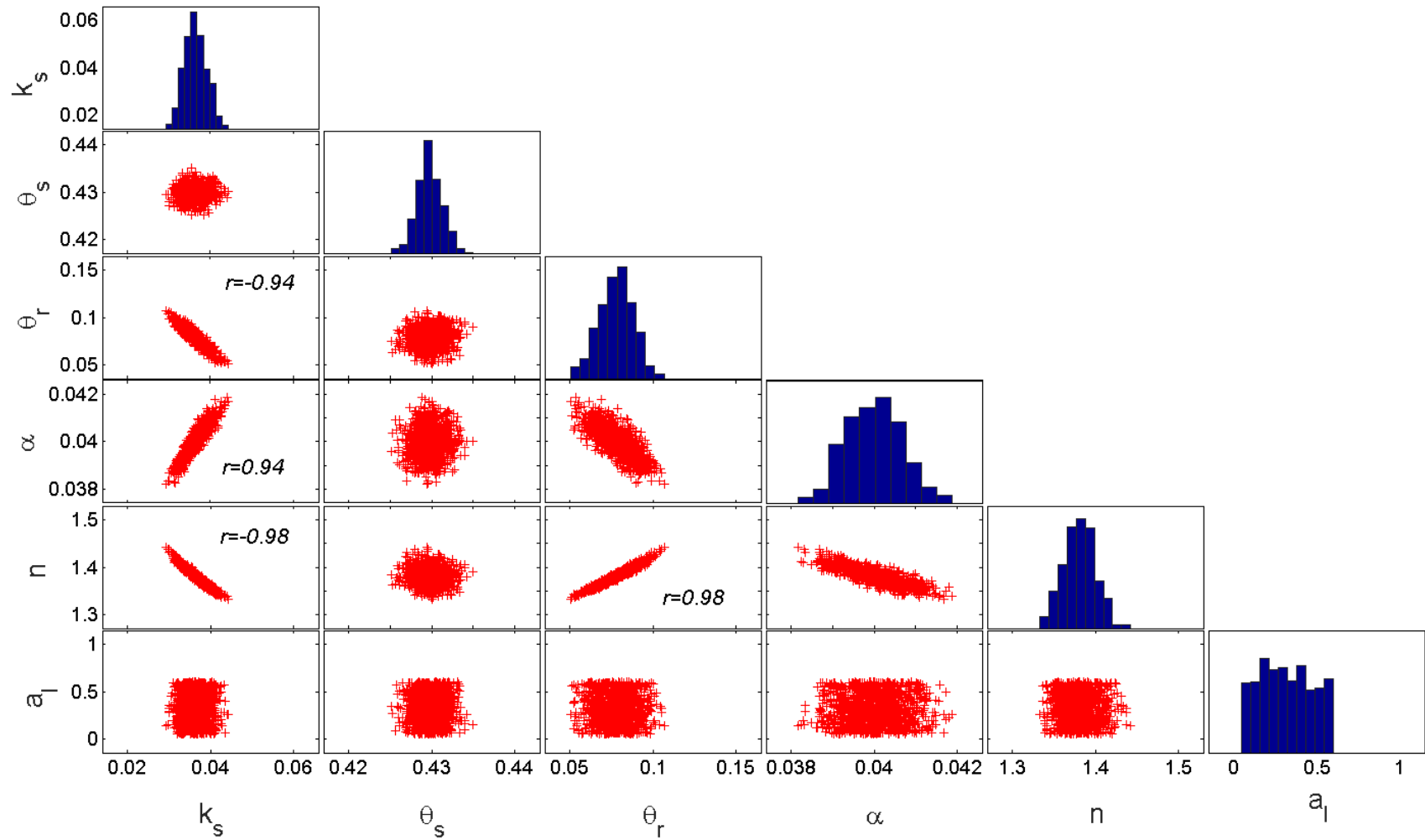


659  
 660  
 661  
 662  
 663  
 664  
 665

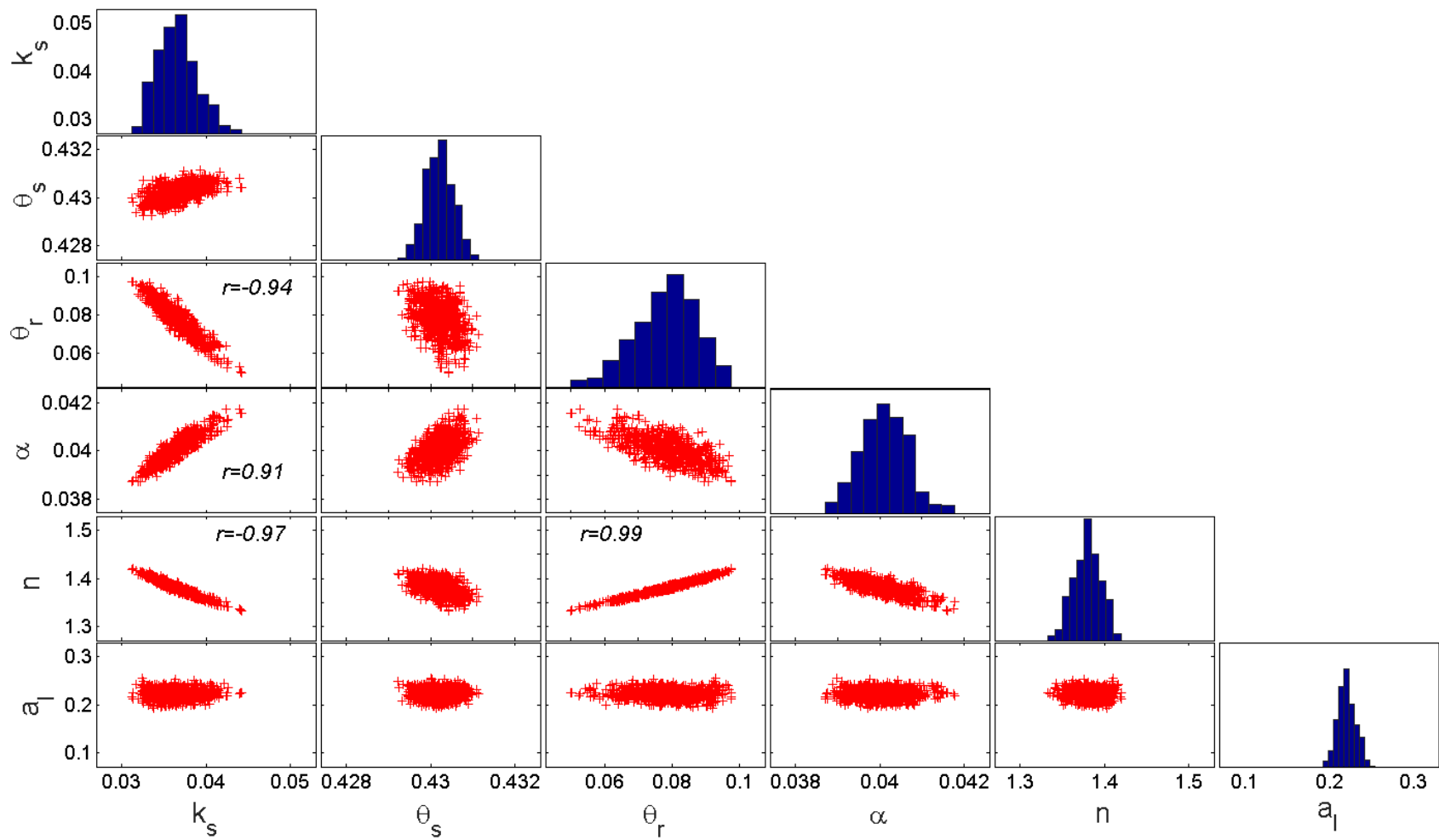
Fig. 1. (a) Pressure head at 5 cm below the soil surface, (b) water content at 5 cm below the soil surface, (c) cumulative outflow, (d) retention curve, (e) output concentration for  $T_{inj} = 5000$  and (f) for  $T_{inj} = 3000$  min. Solid lines represent model outputs and dots represent the sets of perturbed data serving as conditioning information for model calibration.



1  
 2 Fig. 2. MCMC solutions for the transport scenario 1. The diagonal plots represent the inferred posterior probability distribution of the model  
 3 parameters. The off-diagonal scatterplots represent the pairwise correlations  $r$  in the MCMC draws.

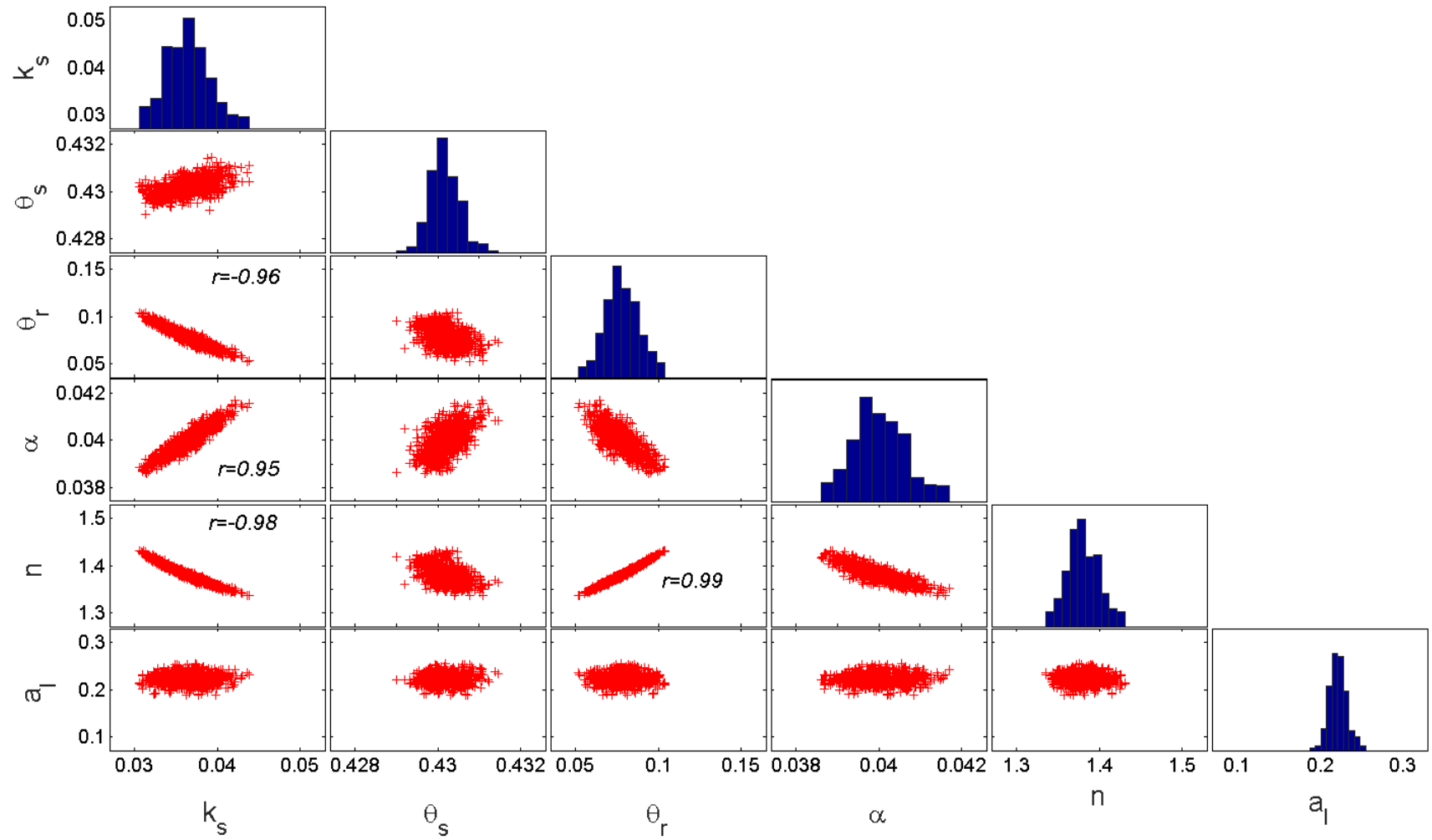


1  
2 Fig. 3. MCMC solutions for transport scenario 2 [see Fig. 2 caption].  
3

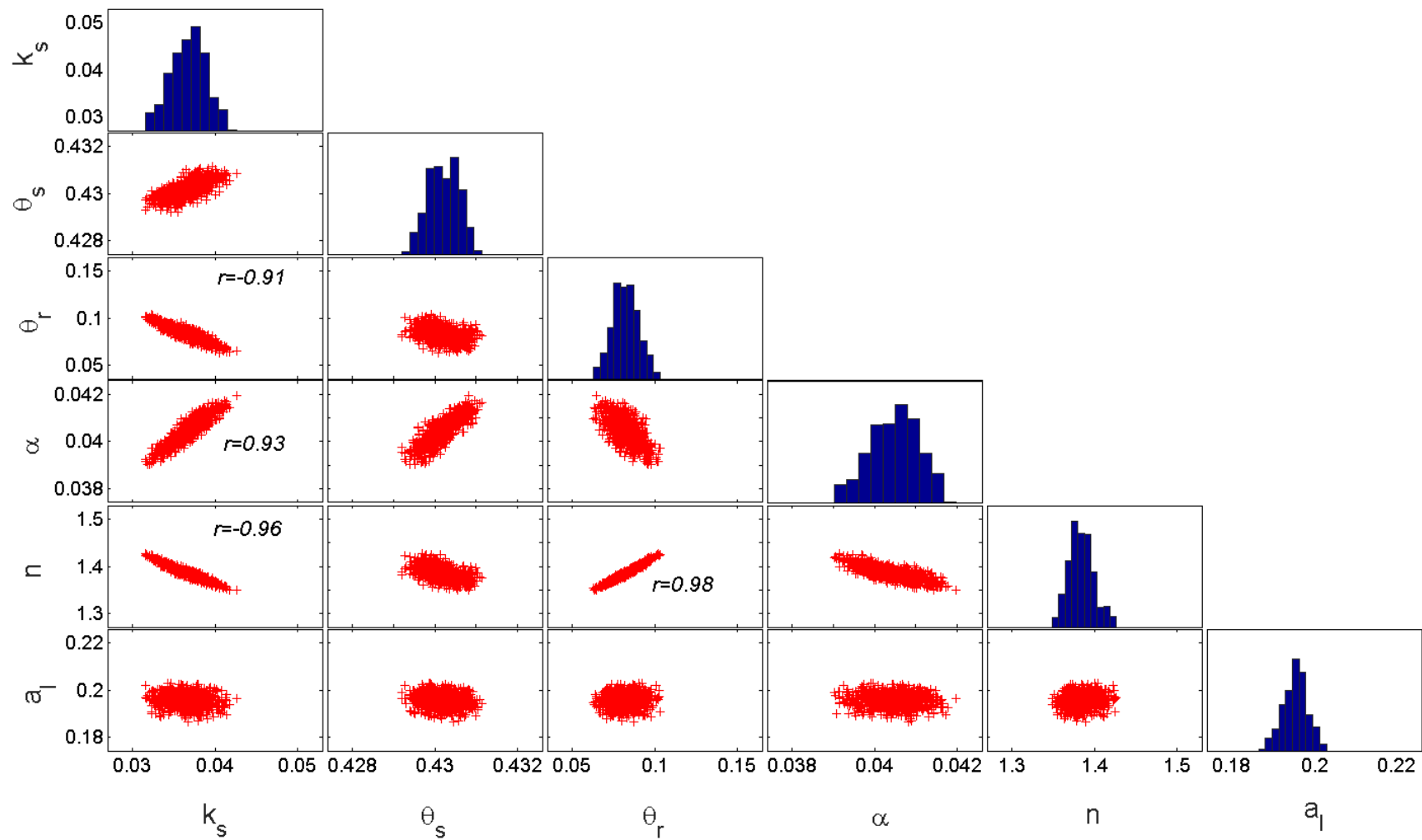


1  
2 Fig. 4. MCMC solutions for transport scenario 3 [see Fig. 2 caption].

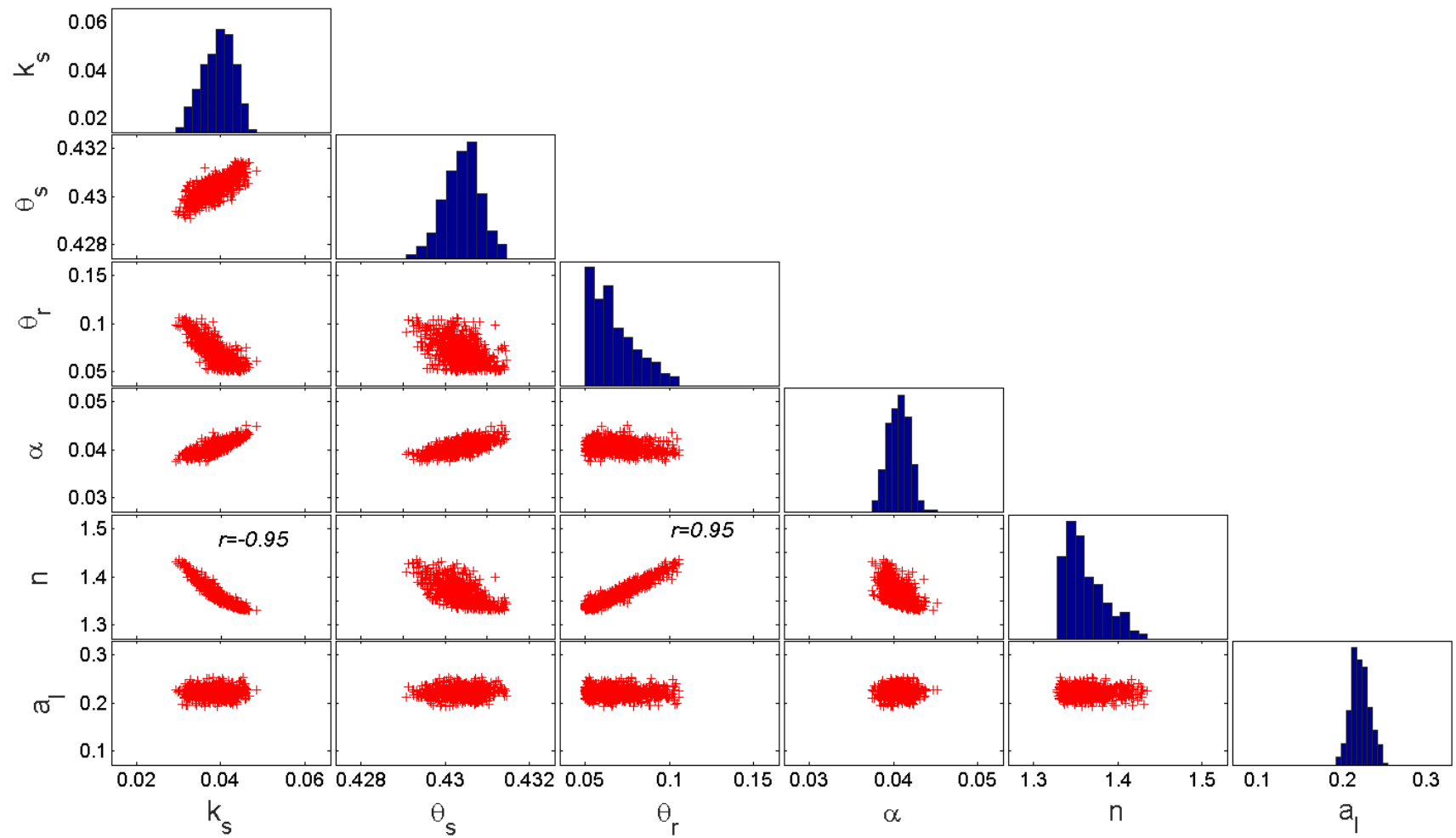




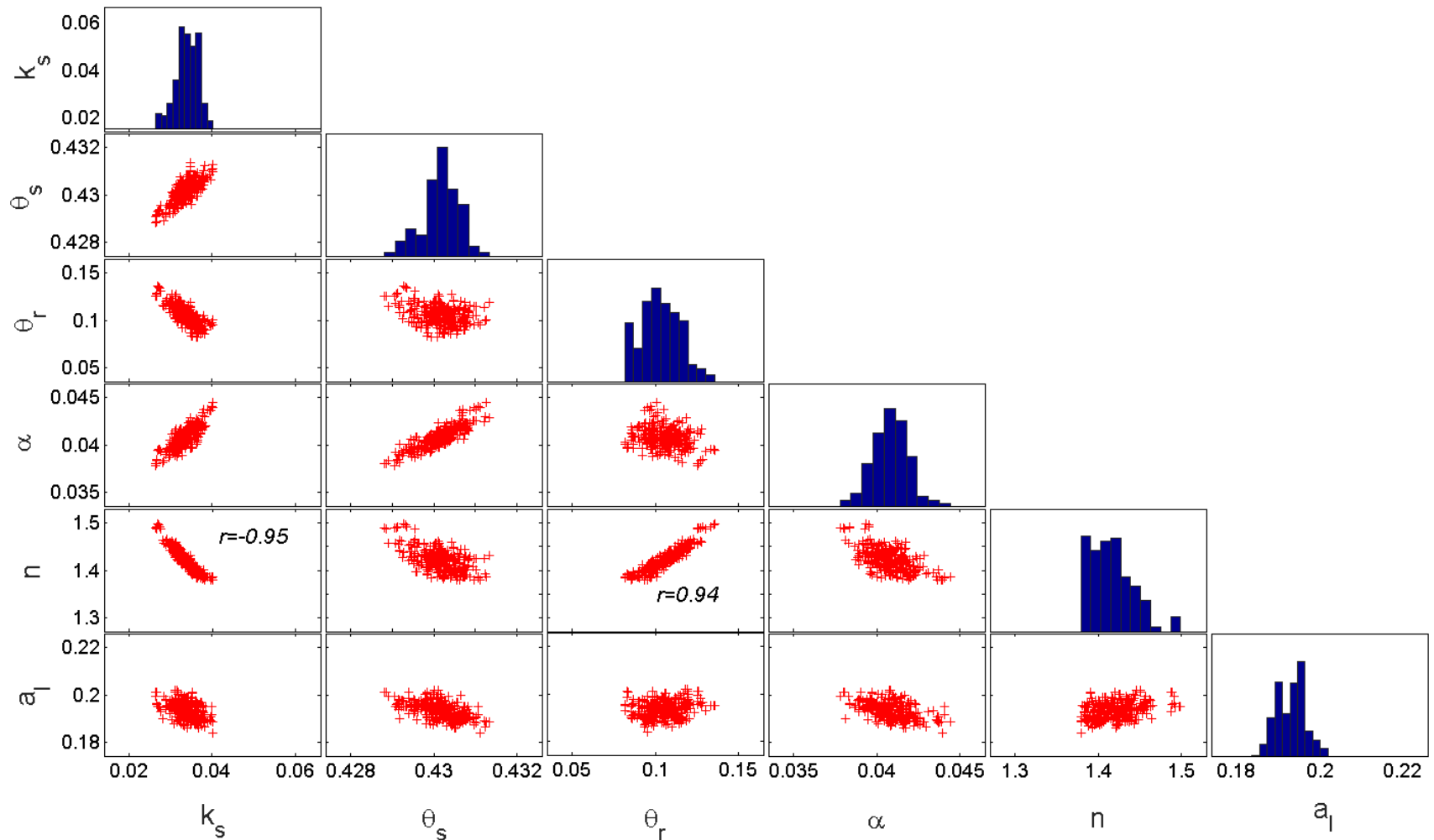
1  
2 Fig. 5. MCMC solutions for transport scenario 4 [see Fig. 2 caption].



1  
2 Fig. 6. MCMC solutions for transport scenario 5 [see Fig. 2 caption].



1  
2 Fig. 7. MCMC solutions for transport scenario 6 [see Fig. 2 caption].



1  
2  
3

Fig. 8. MCMC solutions for transport scenario 7 [see Fig. 2 caption].

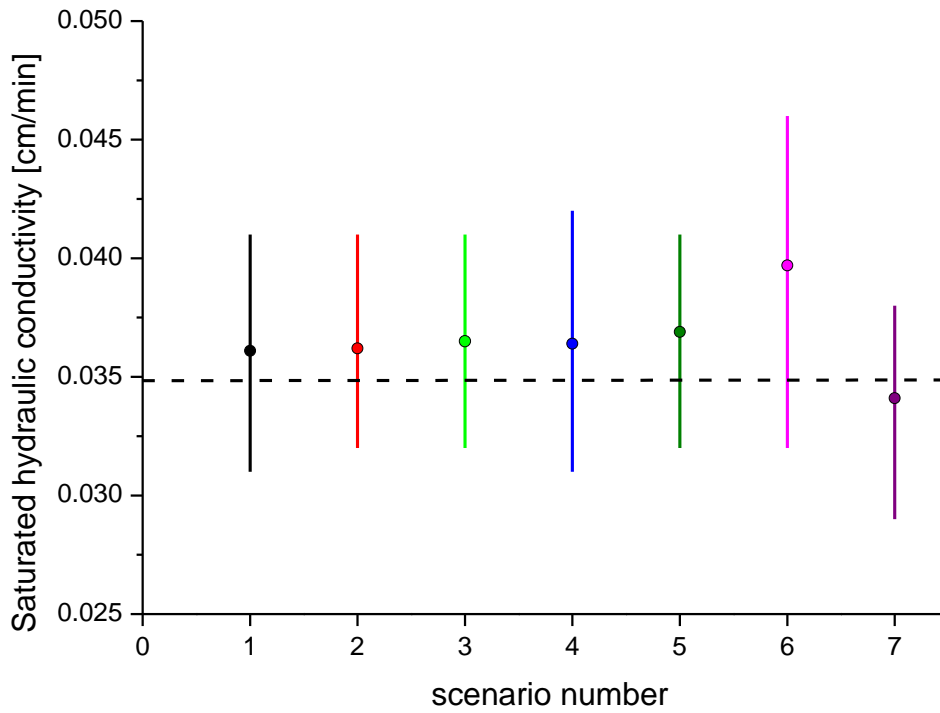


Fig. 9. Posterior mean values and 95% confidence intervals of the saturated hydraulic conductivity for the different scenarios.

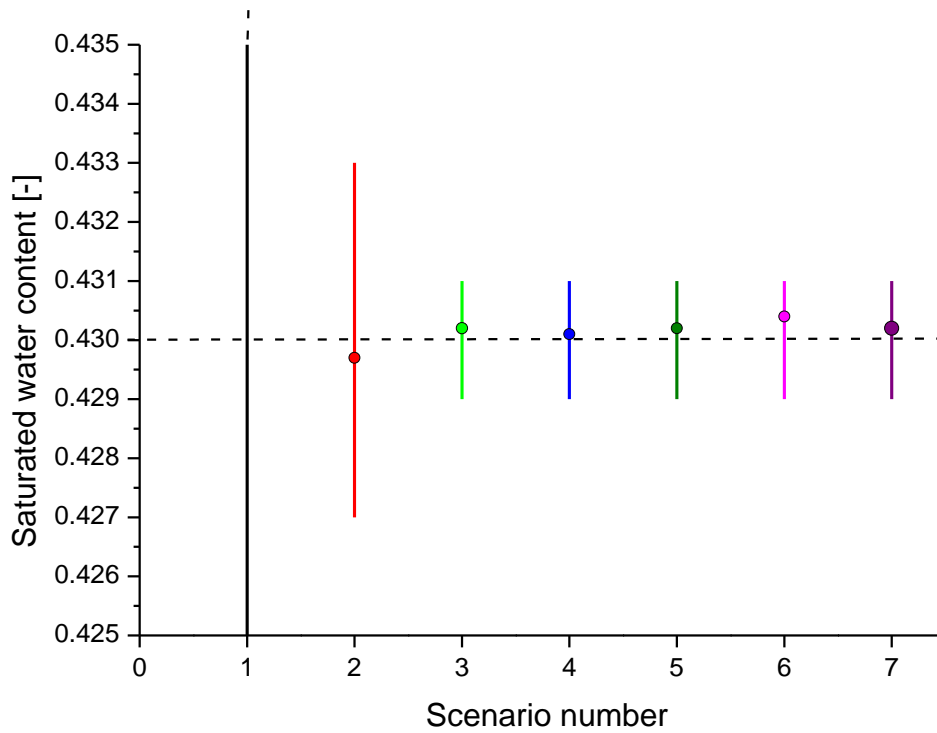


Fig. 10. Posterior mean values and 95% confidence intervals of the saturated water content for the different scenarios.

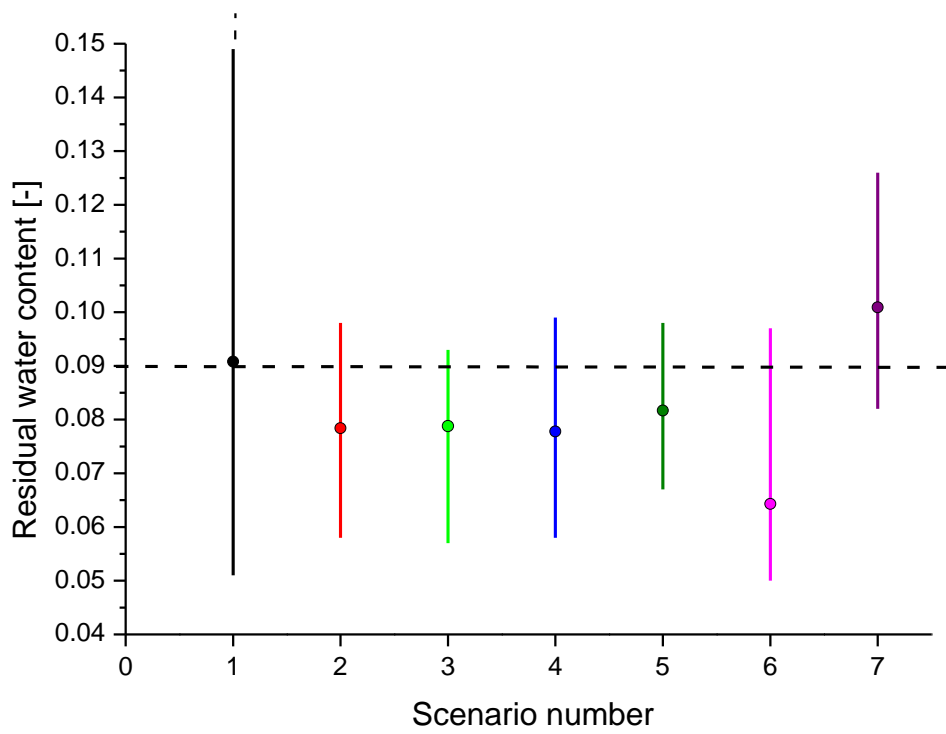


Fig. 11. Posterior mean values and 95% confidence intervals of the residual water content for the different scenarios.

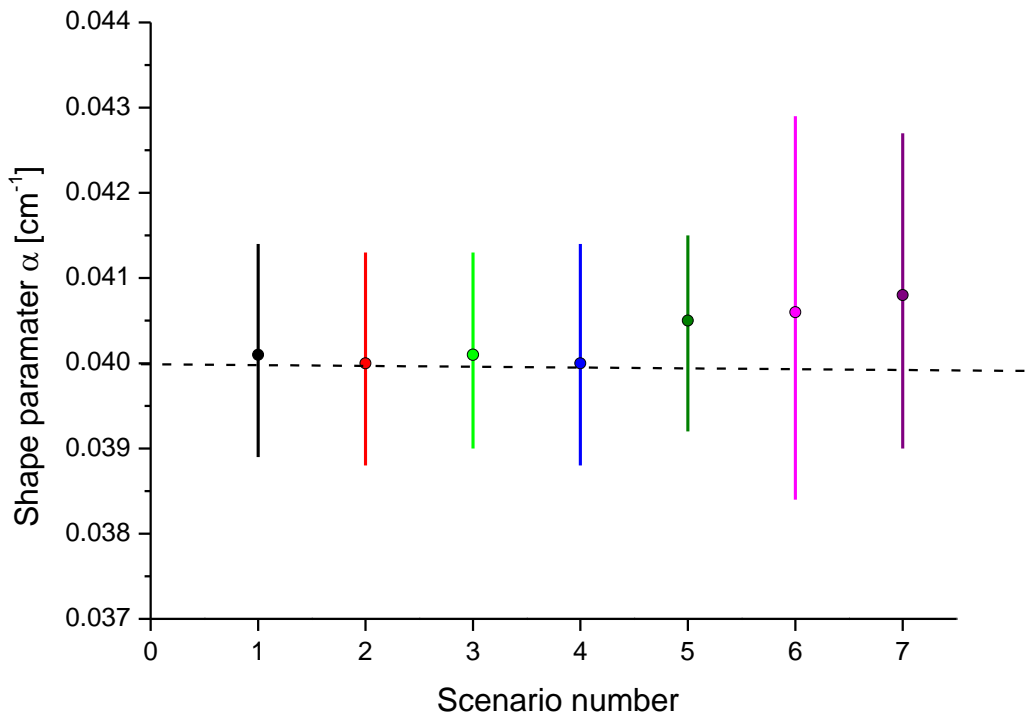


Fig. 12. Posterior mean values and 95% confidence intervals of the shape parameter  $\alpha$  for the different scenarios.

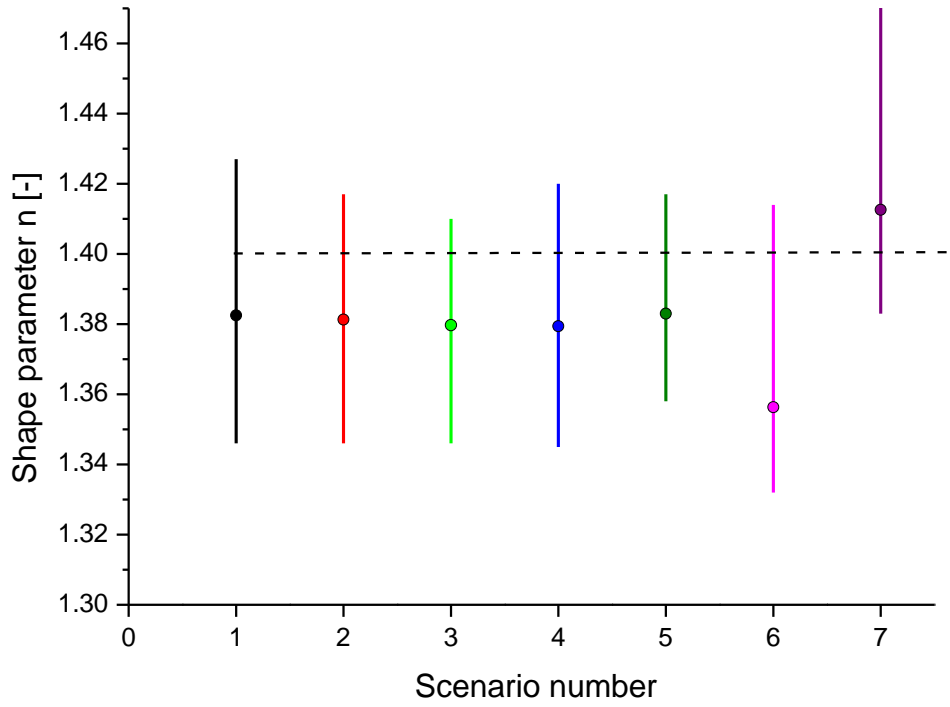


Fig. 13. Posterior mean values and 95% confidence intervals of the shape parameter  $n$  for the different scenarios.

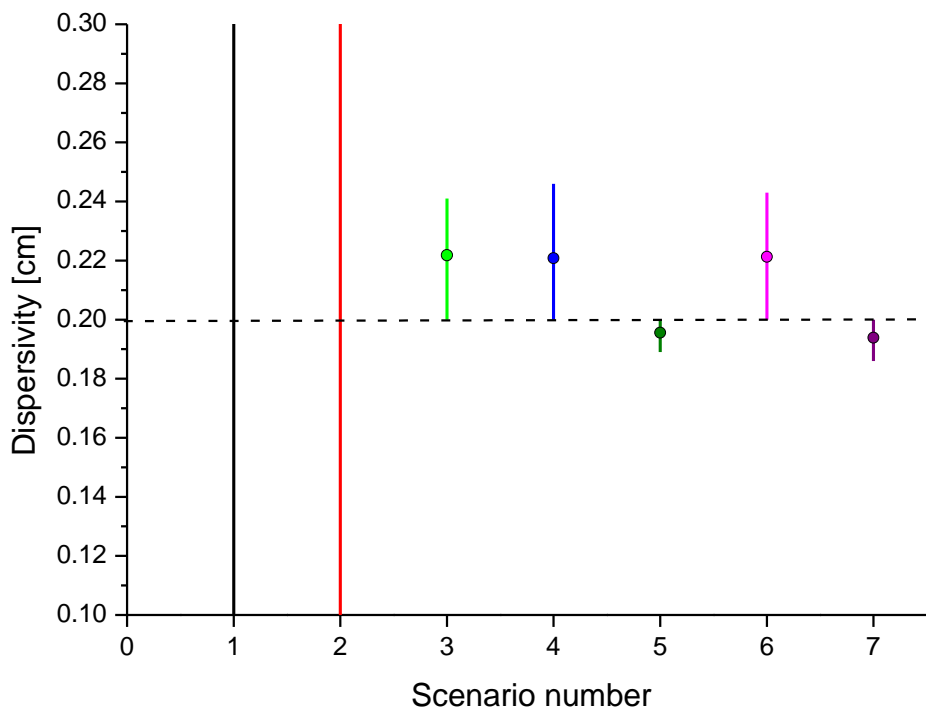


Fig. 14. Posterior mean values and 95% confidence intervals of dispersivity for the different scenarios.